

---

## Local Tchebichef Moments for Texture Analysis

---

Ramakrishnan Mukundan

Orthogonal moment functions based on Tchebichef polynomials have found several applications in the field of image analysis because of their superior feature representation capabilities. Local features represented by such moments could also be used in the design of efficient texture descriptors. This chapter introduces a novel method of constructing feature vectors from orthonormal Tchebichef moments evaluated on  $5 \times 5$  neighborhoods of pixels, and encoding the texture information as a Lehmer code that represents the relative strengths of the evaluated moments. The features will be referred to as Local Tchebichef Moments (LTMs). The encoding scheme provides a byte value for each pixel, and generates a gray-level “LTM-image” of the input image. The histogram of the LTM-image is then used as the texture descriptor for classification. The theoretical framework as well as the implementation aspects of the descriptor are discussed in detail.

---

Ramakrishnan Mukundan  
Department of Computer Science and Software Engineering University of Canterbury  
Christchurch, New Zealand  
e-mail: mukundan@canterbury.ac.nz

## 6.1 Introduction

Moment functions with discrete orthogonal kernels are designed primarily with the aim of deriving improved feature representation capability in pattern analysis applications. When compared with geometric and other types of non-orthogonal moments, discrete orthogonal moments are generally less susceptible to noise and numerical instabilities. While it is theoretically possible to construct moment functions using any class of discrete orthogonal polynomials, we often give importance to simplicity of algebraic structures and the availability of recurrence equations that can be easily implemented. In this context, Tchebichef polynomials have the advantage of being orthogonal functions of unit weight over an integral domain, and having a simple recurrence formula for polynomial computation [6, 22]. Since their introduction in 2001, Tchebichef moments [16, 14] have found several applications in the field of image analysis because of their straightforward definition that allows the computation of orthogonal moments directly in the image coordinate space. Further research in this field has led to the development of more general classes of moments such as the Hahn moments [27] and Krawtchouk moments [26]. Discrete orthogonal moments have also been used in image watermarking [20], face recognition [24], and audio signal compression [8]. Very recently, some research work towards the use of Tchebichef moments for texture classification has been reported [12]. In all these applications, moments are primarily used as global features for representing, recognizing or reconstructing shapes present in the image.

Textures form a special class of images where the shapes present in the images have a high degree of randomness or irregular structures. We cannot therefore use global features that are generally suitable for representing only well-defined and deterministic spatial attributes. For processing textures, we require quantitative measures derived from the spatial arrangement of intensities and any statistical properties they may have. Local features that are obtained using neighborhood operations around each pixel are commonly employed to characterize these variations in the intensity distribution, and for classifying the overall shape features present in images in a statistical sense. The downside of pixel-level processing is that it generates a large amount of per-pixel data with several repetitions or similarities. Hence, the features are usually combined together using their statistical or fractal properties to get a much smaller number of feature descriptors that are both significant and meaningful [13]. Such feature representation methods are commonly used for texture classification, segmentation, and identification of regions of interest [17, 28, 5].

Texture analysis methods play a very important role in the field of medical image analysis. Texture characteristics can be effectively used in discriminating between pathological and normal cases in tissue images and retinal images [9]. Studies have revealed that local intensity operations and related texture features can be used in the analysis of pulmonary emphysema and other disease patterns in lung images [23]. We review some of the commonly used texture analysis methods in the next section.

This chapter introduces Local Tchebichef Moments (LTM) and the associated methods for developing efficient texture feature descriptors. Moment computation is performed in  $5 \times 5$  pixel neighborhoods, so that sufficient information about the local intensity distribution could be captured in a small moment set. Pre-computed con-

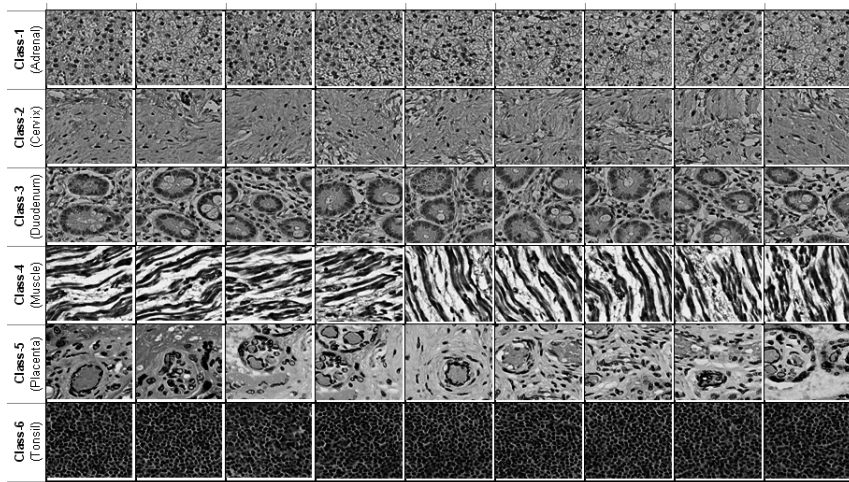


Figure 6.1: A small tissue image database consisting of six different classes of tissue samples.

volution masks are used to evaluate the LTM. The algorithm presented here uses a novel approach of encoding the information about the relative magnitudes of moments in a byte value, producing a gray level map (called the “LTM image”) of the input, and also a texture descriptor in the form of a histogram. The complete framework of this method and its experimental evaluation using a tissue image database are presented. The book chapter is organized as follows. Section 6.2 gives a general overview of the method and compares it with similar approaches that use neighborhood operations and encoding of the resulting information. The computation of orthonormal Tchebichef polynomials using recurrence relations, their general properties and the computation of LTM descriptors using convolution masks are given in Section 6.3. LTM descriptors are introduced in Section 6.4. Section 6.5 gives an example of application of these descriptors in texture classification. Section 6.6 summarizes the main concepts presented in this chapter and also outlines future work.

## 6.2 Texture Feature Descriptors

Irregularity and randomness are the primary shape characteristics seen in most textures. Several types of biomedical images such as tissue microarray images, ultrasound images, high resolution computed tomography (HRCT) images, and digital microscopy images of biopsy samples contain texture-like features at various resolutions. Such features can be used for classifying images based on tissue type, prevalence of disease, or other cytological properties. As an example, a collection of tissue images grouped into six different classes (Adrenal, Cervix, Duodenum, Muscle, Placenta and Tonsil) is shown in Fig.(6.1). We shall use this image database later to test the effectiveness of our feature descriptors in classification.

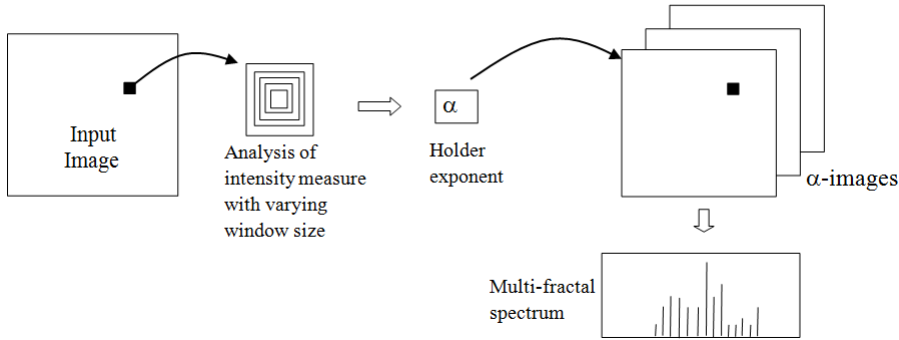


Figure 6.2: An overview of the computation of multifractal spectrum of an image.

The shape features of non-uniform structures present in texture images can be captured through carefully designed quantitative measures which are then combined to form a descriptor using reduction techniques or transformations that retain the essential discriminating statistical features. Several approaches have been used in obtaining such descriptors; an excellent introduction to these methods can be found in [17, 28, 5, 13]. A very popular method is the energy approach developed by Laws [11] that uses nine  $3 \times 3$  convolution masks, and the energy information obtained through the nine channels are combined to form a reduced descriptor for the texture classifier. Another approach for texture interpretation uses the statistical self-similarity properties in textures [4]. A texture image could also be viewed as a superposition of several fractal structures. Multifractal analysis methods decompose an image into a set of disjoint “alfa-images” where each image represents a collection of pixels whose local neighborhoods have similar variation of intensity measure, satisfying the same power law as the window size is increased. The rate at which an intensity measure scales with respect to window size is represented by the Holder exponent ( $\alpha$ ). The fractal dimensions of the  $\alpha$ -images collectively form the multi-fractal spectrum and is used as the main descriptor for texture classification [15, 21]. Figure 6.2 shows the main steps involved in the computation of the multi-fractal spectrum. Multifractal methods can be augmented with multi-scale techniques for improving the discriminating power of the extracted features [25].

Another powerful texture descriptor that has been successfully applied in classification is called the Local Binary Pattern (LBP) [17, 19]. This feature is derived by comparing the intensity at each pixel with its eight neighbors and encoding the information in an 8-bit integer value. This encoding can be viewed as a transformation of the input image into an LBP image as shown in Fig.(6.3). The histogram of the LBP image is used for texture classification. LBP methods have been successfully used in the analysis of disease patterns in HRCT lung images [23].

The method based on local Tchebichef moments presented in this chapter is inspired by Laws’ approach. It uses  $5 \times 5$  convolution masks obtained using Tchebichef polynomials of degree 0 through 4, providing five local Tchebichef moments (LTMs)

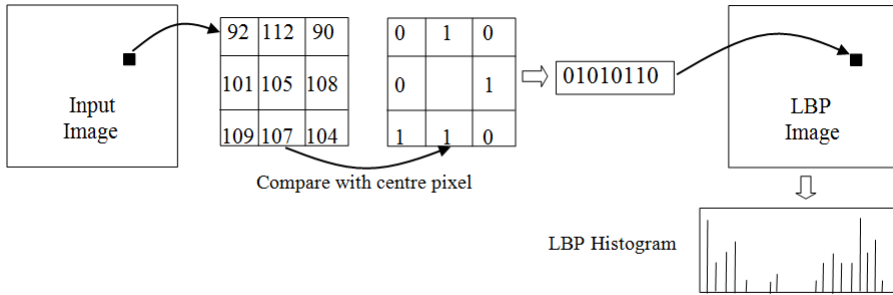


Figure 6.3: An overview of texture processing using the LBP operator.

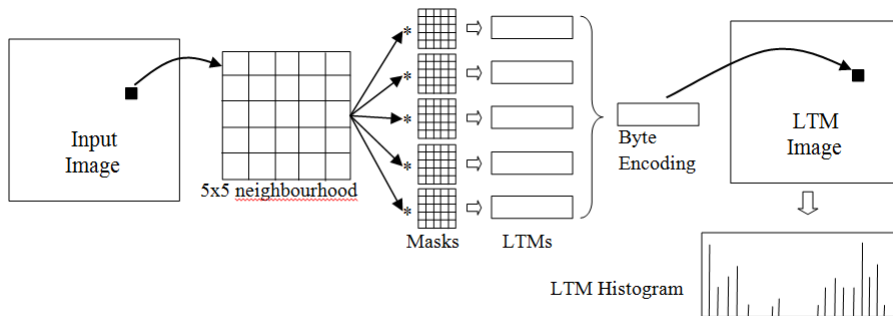


Figure 6.4: A schematic showing different stages of LTM image computation.

for each pixel neighborhood. These moments are then sorted in ascending order, and a unique index denoting the order of moments is computed based on Lehmer code [1]. Since there are 120 possible permutations of five LTMs, the Lehmer code assigns a value between 0 and 119. This value is then multiplied by 2 to get a result in the range 0 to 238. The relative strengths of the five LTMs at each pixel are thus encoded into a single byte value. The collection of byte values gives a gray-level “LTM image”. The histogram values of the LTM image are then used in the classifier. Note that this stage is similar to that used in LBP images. Figure 6.4 gives a schematic of the whole process. The various steps involved in the process are described in detail in the following sections. The next section describes the computation of masks for obtaining local Tchebichef moments.

## 6.3 Local Tchebichef Moments

We use orthonormal Tchebichef polynomials [16] for computing the elements of the convolution masks which give us the associated local moments. We denote orthonor-

mal Tchebichef polynomials of degree  $n$  by  $t_n(x)$ . The polynomials satisfy the following recurrence relation [14]:

$$t_n(x) = \alpha_1 x t_{n-1}(x) + \alpha_2 t_{n-1}(x) + \alpha_3 t_{n-2}(x), \quad (6.1)$$

with  $x = 0, 1, \dots, N-1$ ,  $n = 2, \dots, N-1$  and

$$\begin{aligned} \alpha_1 &= \frac{2}{n} \sqrt{\frac{4n^2 - 1}{N^2 - n^2}}, \\ \alpha_2 &= \frac{(1 - N)}{n} \sqrt{\frac{4n^2 - 1}{N^2 - n^2}}, \\ \alpha_3 &= -\frac{(n-1)}{n} \sqrt{\frac{2n+1}{2n-3}} \sqrt{\frac{N^2 - (n-1)^2}{N^2 - n^2}}. \end{aligned} \quad (6.2)$$

The starting values for the above recurrence can be obtained from the following equations:

$$\begin{aligned} t_0(x) &= \frac{1}{\sqrt{N}}, \\ t_1(x) &= (2x + 1 - N) \sqrt{\frac{3}{N(N^2 - 1)}}. \end{aligned} \quad (6.3)$$

Orthonormal functions have nearly uniform range of values for different values of  $n$ . Plots showing variations of  $t_n(x)$  for different values of  $x$  and  $n$ , with  $N = 5$  are shown in Fig.(6.5).

We can now define elements of  $5 \times 5$  convolution masks  $M_{mn}$  as :

$$M_{mn}(x, y) = t_m(x) t_n(y), \quad m, n, x, y = 0, \dots, 4. \quad (6.4)$$

The values of some of the masks are given as examples in Fig.(6.6) below:

The convolution of a  $5 \times 5$  neighborhood of a pixel at  $(x, y)$  with a mask  $M_{mn}$  directly gives the corresponding local Tchebichef moment (LTM) at location  $(x, y)$ :

$$T_{mn}(x, y) = \sum_{i=0}^4 \sum_{j=0}^4 M_{mn}(i, j) f(x+i-2, y+j-2), \quad m, n = 0, \dots, 4. \quad (6.5)$$

where  $f(x, y)$  denotes the image intensity values. We will not compute all 25 different moment terms given by Eq.(6.5). We will select only a few of the LTMs to represent the local intensity variations and form a feature vector using them as detailed in the next section.

## 6.4 LTM Descriptor

We construct a feature vector consisting of five elements  $\Gamma(x, y) = \{L_i(x, y) : i = 0, \dots, 4\}$ , where each  $L_i$  is a local Tchebichef moment:

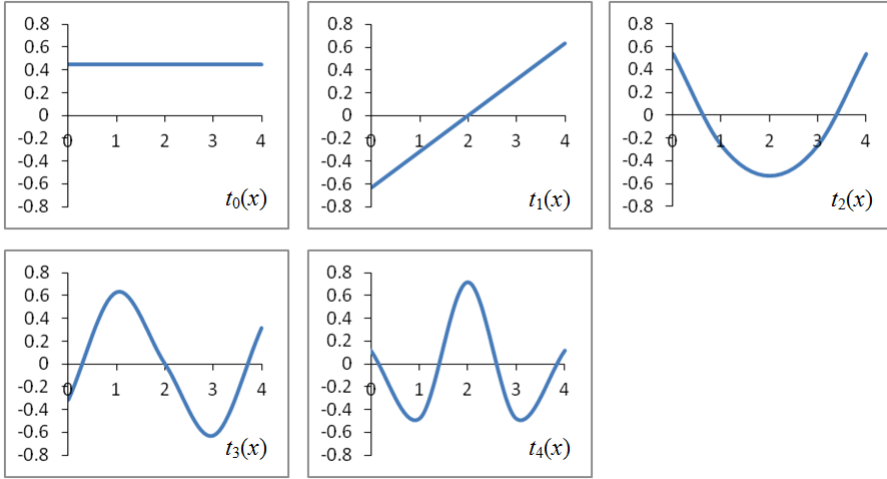


Figure 6.5: Plots of orthonormal Tchebichef polynomials  $t_n(x)$  for  $n = 0$  to  $4$ , and  $N = 5$ .

$$L_i(x, y) = T_{mn}(x, y) \text{ for some } m, n \in [0, 4], i = 0, \dots, 4. \quad (6.6)$$

We can further generalize the above definition allowing for weighted linear combinations of LTMs. For example, we could define our feature vector as

$$\Gamma(x, y) = \{w_0 T_{00}(x, y), w_1 T_{10}(x, y), w_2 T_{01}(x, y), w_3 T_{22}(x, y), w_4 T_{44}(x, y)\} \quad (6.7)$$

or something like

$$\Gamma(x, y) = \{w_0 (T_{00}(x, y) + T_{01}(x, y)), w_1 (T_{21}(x, y) + T_{12}(x, y)), w_2 T_{11}(x, y), w_3 T_{32}(x, y), w_4 T_{33}(x, y)\}, \quad (6.8)$$

where  $w_i$ s are positive weights chosen to give a nearly equal range of variation for all  $L_i$ s. In the most general form, we can write

$$L_i(x, y) = \sum_k (T_{mn})_k w_k, \quad m, n \in [0, 4], i = 0, \dots, 4, w_k > 0, \forall k. \quad (6.9)$$

Even though the five elements of the LTM feature vector can be selected to provide us enough information about the distribution of intensities and their local frequency components, we do not require their actual numerical values. We would like to further encode the information in a single value that uniquely represents the relative strengths

$M_{00}$ 

0.2	0.2	0.2	0.2	0.2
0.2	0.2	0.2	0.2	0.2
0.2	0.2	0.2	0.2	0.2
0.2	0.2	0.2	0.2	0.2
0.2	0.2	0.2	0.2	0.2

 $M_{10}$ 

-0.283	-0.141	0	0.141	0.283
-0.283	-0.141	0	0.141	0.283
-0.283	-0.141	0	0.141	0.283
-0.283	-0.141	0	0.141	0.283
-0.283	-0.141	0	0.141	0.283

 $M_{01}$ 

-0.283	-0.283	-0.283	-0.283	-0.283
-0.141	-0.141	-0.141	-0.141	-0.141
0	0	0	0	0
0.141	0.141	0.141	0.141	0.141
0.283	0.283	0.283	0.283	0.283

 $M_{11}$ 

0.4	0.2	0	-0.2	-0.4
0.2	0.1	0	-0.1	-0.2
0	0	0	0	0
-0.2	-0.1	0	0.1	0.2
-0.4	-0.2	0	0.2	0.4

 $M_{12}$ 

-0.338	-0.169	0	0.169	0.338
0.169	0.085	0	-0.085	-0.169
0.338	0.169	0	-0.169	-0.338
0.169	0.085	0	-0.085	-0.169
-0.338	-0.169	0	0.169	0.338

 $M_{22}$ 

0.286	-0.143	-0.286	-0.143	0.286
-0.143	0.071	0.143	0.071	-0.143
-0.286	0.143	0.286	0.143	-0.286
-0.143	0.071	0.143	0.071	-0.143
0.286	-0.143	-0.286	-0.143	0.286

 $M_{33}$ 

0.1	-0.2	0	0.2	-0.1
-0.2	0.4	0	-0.4	0.2
0	0	0	0	0
0.2	-0.4	0	0.4	-0.2
-0.1	0.2	0	-0.2	0.1

 $M_{44}$ 

0.014	-0.057	0.086	-0.057	0.014
-0.057	0.229	-0.343	0.229	-0.057
0.086	-0.343	0.514	-0.343	0.086
-0.057	0.229	-0.343	0.229	-0.057
0.014	-0.057	0.086	-0.057	0.014

Figure 6.6: A set of  $5 \times 5$  masks constructed using orthonormal Tchebichef polynomials.

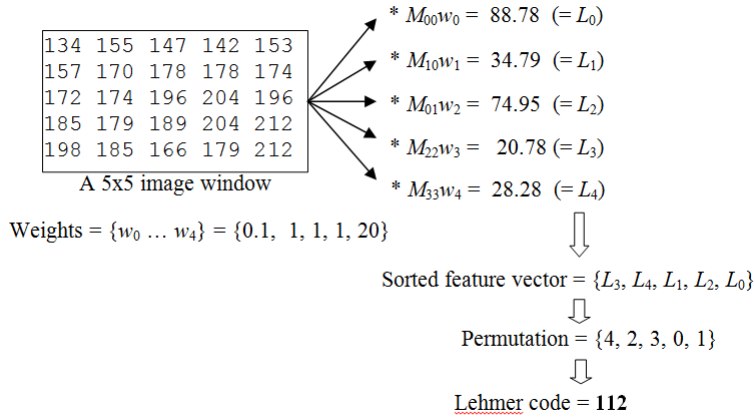


Figure 6.7: An example showing the computation of Lehmer code for a  $5 \times 5$  neighborhood window.

(or “energies”) of the LTM features. Towards this end, we sort the values of  $L_i$  in ascending order, giving a permutation of  $\Gamma(x, y)$ . Since there are  $5! = 120$  permutations possible, we can assign an integer value between 0 and 119 to  $\Gamma(x, y)$  depending on the sequence in which  $L_i$ s appear in the sorted order. This integer value is computed using Lehmer code, and is denoted by  $c(x, y)$ . Figure 6.7 shows the computation of  $c(x, y)$  using an example. Note that this type of encoding is sensitive to minor variations in the numerical values that impact the sorted positions of  $L_i$ . As an example, for a constant image a few of the LTMs are meant to be 0s but their values may actually be stored as  $1.7E - 15$ ,  $0.1E - 16$  etc. These small numerical values will completely alter the sorted order and the final result. One straightforward way to solve this problem is to convert the floating point values of  $L_i$  to nearest integers before sorting them.

When applying  $3 \times 3$  convolution masks, we typically remove the border pixels from the computation as they do not have proper  $3 \times 3$  neighborhoods. In our case, we use  $5 \times 5$  masks and therefore leave out points on a two-pixel wide border around the image. The effect of this will be seen as a black border of the LTM image and a spike at value 0 in its histogram. This problem also can be easily solved by using periodic boundaries (or circular convolution).

We further multiply the computed Lehmer code at each pixel by 2 to expand the range to  $[0, 238]$ , and store the number as a byte value corresponding to the location  $(x, y)$ . The gray-level image thus obtained is the map of the input image under the LTM operator, and will be called the “LTM image”. Figure 6.8 shows the mapping for a sample image using the feature vector and weights shown in Fig.(6.7). The images produced by the Local Binary Pattern (LBP) algorithm [17, 19] and the multifractal analysis method along with their respective feature descriptors are also shown in Fig.(6.8) for comparison.

The histogram of the LTM image will serve as the main descriptor for our classifica-

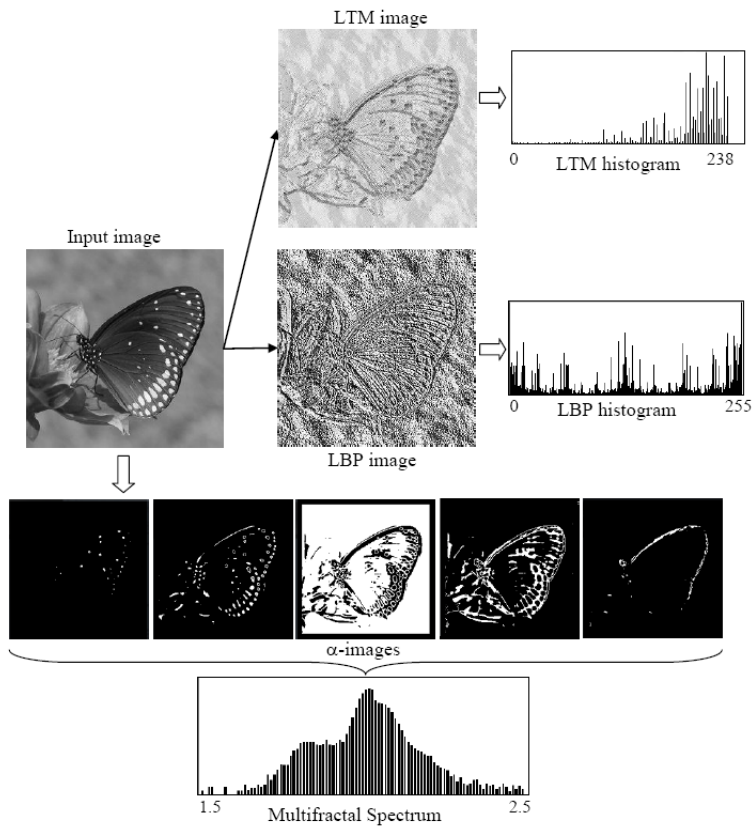


Figure 6.8: A sample image and its LTM-image. For comparison, the LBP image and respective histograms are also shown.

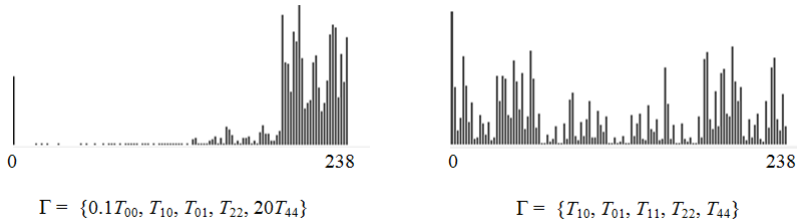


Figure 6.9: Comparison of LTM image histograms for two choices of the feature vector.

tion. In the next section, we will look at the relevant properties or shape attributes of the histogram that can provide sufficient inter-class separability needed for generating accurate results.

It should be noted that the shape of the histogram depends heavily on the choice of moment terms in the feature vector and the corresponding weights. For example, the concentration of points towards the right side of the histogram in Fig.(6.8), shows that the low order moments still dominate the feature set (see Fig.(6.7)). The moment term  $T_{00}$  usually gives a much larger value compared to other terms and therefore was assigned a small weight. If we remove  $T_{00}$  from the feature vector and give uniform weights for all moment terms, then we get a better spread of histogram values as shown in Fig.(6.9). There is always a trade-off between the two choices; on one hand we can have more distinguishing features in the descriptor if the histogram has more values, but on the other hand less number of significant points in the histogram often implies less redundant information in a compact set and therefore faster comparison.

## 6.5 Texture Classification

In this section, we consider the problem of texture classification using LTM descriptors. We first look at intra-class similarity and inter-class variance of the feature descriptors provided by the LTM histogram. The tissue image database shown in Fig.(6.1) will be used for our analysis. Three images from each class in Fig.(6.1) were randomly selected to form the “training set”. The feature vector and weights as given in Fig.(6.7) were used for obtaining the LTM images. The LTM histograms of the complete training set are shown in Fig.(6.10).

The histograms given in Fig.(6.10) show excellent intra-class similarity. This is one of the most desirable features of texture descriptors. Some samples in the test data set do not show significant inter-class differences (eg., Test Data 2 of classes 1 and 3 look very similar) and the corresponding tissue images do not have many statistically separable features. Images belonging to classes 4 and 6 are distinctly different from those belonging to other classes, and this aspect is clearly reflected in the LTM histograms. However, Class 4 is characterized by the fact that the histogram values vary largely within the class leading to classification errors.

As a brute-force method of classification, the average of histogram values  $H_E(i)$

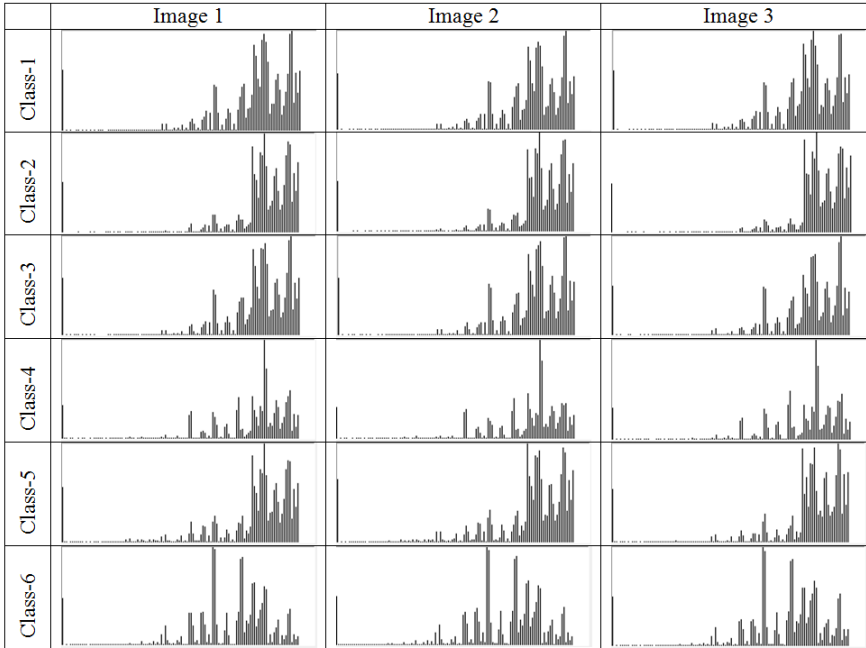


Figure 6.10: LTM image histograms for the test cases from the tissue image database.

obtained from the three images in the training data set were computed for each class, and compared with the LTM histograms  $H_T(i)$  of all test images in Fig.(6.1) using the normalized sum of absolute differences as the similarity measure:

$$D_1(H_T, H_E) = \sum_{i=128}^{238} \left( \frac{|H_T(i) - H_E(i)|}{H_E(i)} \right). \quad (6.10)$$

The standard Chi-square test [7, 10] is also found to yield good results in histogram comparison:

$$D_2(H_T, H_E) = \sum_{i=128}^{238} \left( \frac{(H_T(i) - H_E(i))^2}{H_E(i)} \right). \quad (6.11)$$

Since the histograms contain significant values only on the right half in all cases, only values in the range [128, 238] were used in the comparison (this range will of course depend on the choice of the feature vector as shown in Fig.(6.9)). The classification results obtained using this method are given as a confusion matrix in Table 6.1 below.

The above results compare well with the previously published classification errors for the same database using multifractal measures [15]. The approach taken in that paper used features extracted from the multifractal spectrum of the images as opposed to LTM histograms. For the purpose of comparison, the table given in Fig.(8b) of [15] that gave the best results, is reproduced below (Table 6.2).

Table 6.1: The confusion matrix showing the results of the classification experiment using the tissue database in Fig.(6.1), and LTM image histograms as feature descriptors.

		Predicted					
		Class-1	Class-2	Class-3	Class-4	Class-5	Class-6
Actual	Class-1	88.89	0	11.11	0	0	0
	Class-2	0	77.78	22.22	0	0	0
	Class-3	0	0	100	0	0	0
	Class-4	55.56	0	0	44.44	0	0
	Class-5	0	0	0	0	100	0
	Class-6	0	0	0	0	0	100

Table 6.2: The confusion matrix showing the results of the classification experiment using the tissue database in Fig.(6.1), and features based on multifractal spectra [15].

		Predicted					
		Class-1	Class-2	Class-3	Class-4	Class-5	Class-6
Actual	Class-1	100	0	0	0	0	0
	Class-2	0	88.89	11.11	0	0	0
	Class-3	0	0	100	0	0	0
	Class-4	0	0	22.22	77.78	0	0
	Class-5	0	11.11	0	0	88.89	0
	Class-6	0	0	0	0	0	100

The results given in Table 6.1 could be further improved by carefully selecting the LTMs in the feature vector using a rigorous analysis of the intensity moments for the given dataset (domain knowledge), and using robust similarity measures [2] for obtaining accurate histogram matching. Biomedical image classification algorithms often use more advanced classifiers such as K-nearest neighbors and support vector machines [3], that could also provide better results. The primary aim of this book chapter was to introduce the framework for local Tchebichef moments, and therefore detailed optimization aspects have been left out.

## 6.6 Summary

A feature set constructed using discrete orthogonal moments based on Tchebichef polynomials can effectively represent the intensity distribution within an image window. This property is utilized in developing a local moment operator that provides a feature vector at each pixel location. Such operators can be easily implemented as convolution masks designed for a reasonably sized pixel neighborhood. For texture analysis applications, the local Tchebichef moments can be combined into a byte value by using Lehmer codes for the sorted permutation of the feature vector. The byte values define a mapping of the input image to the LTM-image. The histogram of this image can then be used as the feature descriptor. This book chapter provided the framework for this novel algorithm, and also presented experimental results showing the potential of the method in applications such as texture feature representation and classification.

Future research work using LTM descriptors can take several directions. One could analyse the properties of the computed features in moment space to determine the optimal set and weights (Eq.(6.9)) that should be used as the feature vector for a given application. This research can be combined with an analysis of the primary features that should be selected from the LTM histogram for classification. Another aspect that needs to be considered, specially for texture recognition applications, is the invariance of the feature descriptor under both spatial and intensity transformations. The possibility of combining the LTM descriptor with global image moments for improving the classification accuracy could also be looked at. For example, images in Class-4 (Fig.(6.1)) have a global image shape that is distinctly different from other images. The use of global moments could reduce the classification error seen in Table 6.1. Methods that combine local and global descriptors are increasingly being used in texture analysis. Papakostas et. al., [18] recently introduced moment-based LBP descriptor that combines the properties of locality, globality and invariance. Finally, the discrimination power of the proposed LTM descriptors could be further improved by selecting the free parameters using proper optimization methods such as the evolutionary algorithm.

## References

- [1] J. Arndt. *Matters Computational – Ideas, Algorithms, Source Code*. Springer, 2011.

- [2] S.H. Cha and S.N. Srihari. On measuring the distance between histograms. *Pattern Recognition*, 35(6), 2002.
- [3] E. Cheng, N. Xie, H. Ling, P.R. Bakic, A.D.A. Maidment, and V. Megalooikonomou. Mammographic image classification using histogram intersection. In *IEEE International Symposium on Biomedical Imaging: From Nano to Macro (ISBI)*, pages 197–200, April 2010.
- [4] A.F. Costa, G. Humpire-Mamani, and J.M.A. Traina. An efficient algorithm for fractal analysis of textures. In *Conference on Graphics, Patterns and Images (SIBGRAPI)*, pages 39–46, August 2012.
- [5] E.R. Davies. Introduction to texture analysis. In M. Mirmehdi, X. Xie, and J. Suri, editors, *Handbook of Texture Analysis*. World Scientific, 2008.
- [6] W. Gautschi. *Orthogonal Polynomials: Computation and Approximation*. Oxford University Press, 2004.
- [7] S.G. Hoggar. *Mathematics of Digital Images*. Cambridge University Press, 2006.
- [8] W.A. Jassim, P. Raveendran, and R. Mukundan. New orthogonal polynomials for speech signal and image processing. *IET Signal Processing*, 6(8):713–723, 2012.
- [9] V.K. Jestin, J. Anitha, and D.J. Hemanth. Textural feature extraction for retinal image analysis. In *International Conference on Computing, Electronics and Electrical Technologies (ICCEET)*, pages 548–551, March 2012.
- [10] R. Laganiere. *OpenCV 2 Computer Vision Application Programming Cookbook*. Packt Publishing, 2011.
- [11] K.I. Laws. Rapid texture identification. In *SPIE, Image Processing for Missile Guidance*, volume 238, pages 376–380, 1980.
- [12] J.V. Marcos and G. Cristobal. Texture classification using discrete Tchebichef moments. *J. Opt. Soc. Am. A*, 30(8):1580–1591, 2013.
- [13] K. Mikolajczyk and C. Schmid. A performance evaluation of local descriptors. *IEEE Transactions on Pattern Analysis and Machine Intelligence*, 27(10):1615–1630, 2005.
- [14] R. Mukundan. Some computational aspects of discrete orthonormal moments. *IEEE Transactions on Image Processing*, 13(8):1055–1059, 2004.
- [15] R. Mukundan and A. Hemsley. Tissue image classification using multifractal spectra. In *Methods and Innovations for Multimedia Database Content Management*, volume 1, pages 61–74. IGI Publishing, 2010.
- [16] R. Mukundan, S.H. Ong, and P.A. Lee. Image analysis by Tchebichef moments. *IEEE Transactions on Image Processing*, 10(9):1357–1364, 2001.
- [17] T. Ojala, M. Pietikäinen, and D. Harwood. A comparative study of texture measures with classification based on featured distributions. *Pattern Recognition*, 29(1):51–59, 1996.
- [18] G.A. Papakostas, D.E. Koulouriotis, E.G. Karakasis, and V.D. Tourassis. Moment-based local binary patterns: A novel descriptor for invariant pattern recognition applications. *Neurocomputing*, 99:358–371, 2013.
- [19] M. Pietikainen, G. Zhao, A. Hadid, and T. Ahonen. *Computer Vision Using Local Binary Patterns*. Springer-Verlag, London, 2011.
- [20] R. Prasad and S.V. Dhavale. Scaling and translation resistant Tchebichef moments in image watermarking. In *International Conference on Information and Network Technology (ICINT)*, volume 37, pages 55–61, 2012.

- [21] I.S. Reljin and B.D. Reljin. Fractal geometry and multifractals in analyzing and processing medical data and images. *Archive of Oncology*, 10(4):283–293, 2002.
- [22] G. Sansone. *Orthogonal Functions*. Dover Publications, 2004.
- [23] L. Sorensen, S.B. Shaker, and M. de Bruijne. Quantitative analysis of pulmonary emphysema using Local Binary Patterns. *IEEE Transactions on Medical Imaging*, 29(2):559–569, 2010.
- [24] D. Sridhar and I.V. Murali Krishna. Face recognition using Tchebichef moments. *International Journal of Information and Network Security*, 1(4):243–254, 2012.
- [25] Y. Xu, X. Yang, H. Ling, and H. Ji. A new texture descriptor using multifractal analysis in multi-orientation wavelet pyramid. In *IEEE Conference on Computer Vision and Pattern Recognition (CVPR)*, pages 161–168, 2010.
- [26] P.T. Yap, R. Paramesran, and S.H. Ong. Image analysis by Krawtchouk moments. *IEEE Transactions on Image Processing*, 12(11):1367–1377, 2003.
- [27] P.T. Yap, R. Paramesran, and S.H. Ong. Image analysis using Hahn moments. *IEEE Transactions on Pattern Analysis and Machine Intelligence*, 29(11):2057–2062, 2007.
- [28] J. Zhang, M. Marszalek, S. Lazebnik, and C. Schmid. Local features and kernels for classification of texture and object categories: A comparative study,. *International Journal of Computer Vision*, 73(2):213–238, 2007.